NOTE

Magnetic Resonance in Medicine 00:00–00 (2014)

SHARP Edges: Recovering Cortical Phase Contrast Through Harmonic Extension

Ryan Topfer,[1] Ferdinand Schweser,[2,3] Andreas Deistung,[2] Jürgen R. Reichenbach,[2] and Alan H. Wilman[1]*

Purpose: To recover local phase contrast at the edges of the brain (e.g., cortex), where it is otherwise unavailable with the conventional form of the technique sophisticated harmonic artifact reduction for phase data (SHARP).

Methods: A harmonic potential field, such as the magnetic "background" field, is an analytic field and can thus be represented by a convergent power series. Using SHARP to obtain an initial estimate of the harmonic background field over a reduced inner portion of the brain, a three-dimensional Taylor expansion was performed to extend field coverage to the brain edges. The method, called *Extended*-SHARP, was quantitatively assessed through a numerical field-forward simulation and qualitatively demonstrated in vivo.

Results: Using a typical spherical kernel (6 mm radius), Extended-SHARP recovered on average 26% more in vivo brain volume than SHARP. When applied to the numerical model, local field contrast around an otherwise lost edge source was recovered, with the resulting error comparable to that of conventional SHARP.

Conclusion: The lost field values near the edges of the brain can be recovered through an easily implemented adaptation to conventional SHARP. **Magn Reson Med 000:000–000, 2014.**

Key words: phase imaging; harmonic extension; SHARP; susceptibility mapping

INTRODUCTION

Susceptibility-related MRI phase contrast has long found clinical application in the form of the well-established susceptibility-weighted imaging (SWI) technique (1–5). Recently, efforts in this field have been increasingly directed toward quantitative susceptibility mapping (QSM), which seeks to collapse the blooming field distortions (a nonlocal and indirect effect) into the underlying material susceptibility itself (6–11). QSM may benefit our understanding of an array of neurodegenerative disorders for which paramagnetic iron is thought to play a role (12), hence, there exists considerable interest in improving the techniques for processing the requisite phase data.

Although the complete set of mechanisms at work in the generation of in vivo phase contrast may not yet be fully understood, it may be stated (albeit, somewhat simplistically) that the magnetic field perturbation and, equivalently, the MR phase scale with change in apparent susceptibility. Whereas intertissue variations in apparent susceptibility (inducing *local field*) deviate only slightly from the bulk susceptibility of water at body temperature, the difference between tissue and air is comparatively dramatic (13), inducing a *background field* which tends to obscure the small-scale field variation of interest.

Two novel approaches to eliminating the background field have recently been published: sophisticated harmonic artifact reduction for phase data (SHARP) (14) and projection onto dipole fields (PDF) (7,15). Unlike traditional high-pass filtering (2), which was based on the empirical observation that the measured phase is to some extent differentially composed of low and high spatial frequencies (contributed by the background and the local fields, respectively), SHARP and PDF look to the underlying physics for an approach which is less heuristic and less dependent on the particular form of the data. Recognizing the measured field as a superposition of local and background fields, SHARP uses the spherical mean value theorem to extract the harmonic background field. On the other hand, PDF makes use of the approximate orthogonality between local and background fields, which, through the Hilbert projection theorem, designates a particular susceptibility distribution, in turn used to model the background field through a field-forward calculation (16,17).

Each method has its own advantages and disadvantages. Of particular importance is that both methods necessitate a definition (i.e., binary input image) of the brain boundary, and both tend to produce invalid results in its vicinity, thereby limiting their application to an internal subsection of tissue. This shared pitfall is a considerable obstacle to several clinical applications as it precludes analysis of features such as pial vessels, cortical dysplasia, subdural hematoma, and cortical lesions in pathologies such as multiple sclerosis.

To recover local field across the edges of the brain, this study presents an extension to conventional SHARP whereby another fundamental property of the background field is used: namely, its analyticity (18,19). The method, *extended*-SHARP (E-SHARP), is quantitatively assessed through a numerical field-forward experiment

[1]Department of Biomedical Engineering, University of Alberta, Edmonton, Alberta, Canada.

[2]Medical Physics Group, Institute of Diagnostic and Interventional Radiology I, Jena University Hospital - Friedrich Schiller University Jena, Germany.

[3]Currently at: Department of Neurology, School of Medicine and Biomedical Science, University of Buffalo, The State University of New York, Buffalo, New York, USA.

Grant sponsors: Canadian Institutes of Health Research (CIHR, MOP 102582), Natural Sciences and Engineering Research Council of Canada (NSERC, 327723), and German Research Foundation (DFG, RE 1123/9-2).

*Correspondence to: Alan H. Wilman, Ph.D., Department of Biomedical Engineering, University of Alberta, 1098 Research Transition Facility, Edmonton, Alberta, T6G 2V2, Canada. E-mail: wilman@ualberta.ca

Drs. Reichenbach and Wilman contributed equally to this work.

Received 8 September 2013; revised 23 December 2013; accepted 4 January 2014

DOI 10.1002/mrm.25148

Published online 00 Month 2014 in Wiley Online Library (wileyonlinelibrary.com).

and qualitatively demonstrated on in vivo human brain data acquired at 4.7 T.

THEORY

Physical principles behind SHARP have been addressed in previous publications (14,20). Beginning with the unwrapped phase and dividing by $\gamma B_0 TE$ (where γ is the proton gyromagnetic ratio, B_0 the strength of the applied field, and TE the echo time) yields an estimate of the relative field perturbation $B^{\Delta}(r)$ along the direction of the applied field. This quantity can be understood as a superposition of fields owing to different sources:

$$B^{\Delta}(r)=B_{\text{local}}(r)+B_{\text{bkgr}}(r)+n(r) \quad [1]$$

Here, n includes anything present in the measurement which is unrelated to susceptibility (e.g., flow effects (2), noise (21), receiver offsets (22), chemical shift (23), contributions from macromolecule proton exchange (24–26), etc.). B_{local} and B_{bkgr} are, respectively, the fields due to magnetic susceptibility variation occurring inside and outside of the volume of interest (VOI, i.e., brain). Starting from Maxwell's equations, it can be shown (20) that, in the absence of noise and susceptibility variation, the static magnetic induction B is harmonic (i.e., satisfies Laplace's equation: $\nabla^2 B = 0$). In other words, B_{bkgr} is harmonic within the VOI.

To eliminate B_{bkgr}, SHARP invokes the spherical mean value (SMV) property: the mean of a harmonic function calculated over a spherically symmetric surface is equal to the value of the function at the center of the sphere (27). However, the SMV cannot be used to estimate the background field wherever the sphere overlaps the edge of the data support. Hence, in conventional SHARP, voxels in this region of overlap are wholly discarded (i.e., set to zero before the deconvolution stage). We refer to these discarded voxels as *edge points* (EP). The collection of voxels retained subsequent to the application of SHARP will be referred to as the *reduced VOI*.

Fortunately, because the background field is harmonic, it is also, necessarily, analytic (18). This means that within a neighborhood of location r_0, for which $B_{\text{bkgr}}(r_0+d)$ is everywhere harmonic, the background field can be expressed as a convergent power series. Practically speaking, given an SMV estimate of $B_{\text{bkgr}}(r_0)$ (i.e., that provided by conventional SHARP), because $B_{\text{bkgr}}(r_0+d)$ is entirely harmonic within the region circumscribed by the SHARP kernel with radius $R=|r_0+d|$ a three-dimensional (3D) Taylor expansion can be performed to extend the field coverage to the hitherto lost EP voxels:

$$B^{\text{EP}} = B^{\text{IP}} + \begin{bmatrix} d_x & d_y & d_z \end{bmatrix} \begin{bmatrix} B_x^{\text{IP}} \\ B_y^{\text{IP}} \\ B_z^{\text{IP}} \end{bmatrix} + \frac{1}{2!} \begin{bmatrix} d_x & d_y & d_z \end{bmatrix} \begin{bmatrix} B_{xx}^{\text{IP}} & B_{xy}^{\text{IP}} & B_{xz}^{\text{IP}} \\ B_{yx}^{\text{IP}} & B_{yy}^{\text{IP}} & B_{yz}^{\text{IP}} \\ B_{zx}^{\text{IP}} & B_{zy}^{\text{IP}} & B_{zz}^{\text{IP}} \end{bmatrix} \begin{bmatrix} d_x \\ d_y \\ d_z \end{bmatrix} + \cdots \quad [2]$$

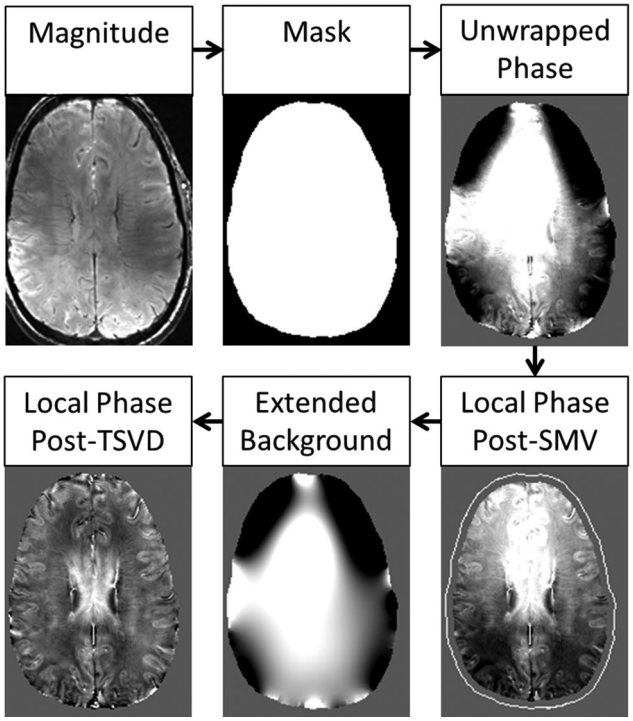

FIG. 1. Simplified work flow. Magnitude data is passed to FSL's brain extraction tool (35), the output of which (*mask*) is used to constrain the unwrapping to the tissue of interest. The SMV kernel is applied to the unwrapped phase and deconvolved without regularization to produce the initial local phase estimate (*local phase post-SMV*). The outline indicates the edge of the mask (VOI) and the edge region lost in conventional SHARP. This local estimate is subtracted from the unwrapped total phase to produce an estimate of the background phase over the reduced VOI (not shown). The Taylor expansion (Eq. [2]) is used to recover the edge voxels (*extended background*). The result is subtracted out from the unwrapped total and SHARP-regularized to produce the final *local phase post-TSVD*.

Here, B^{IP} denotes the background field at an *internal point* (IP) within the reduced VOI; B^{EP} denotes the background field of an EP voxel; B_i^{IP} denotes the first-order derivative in direction i $(i=x,y,z)$ of the background field evaluated at an IP voxel and B_{ij}^{IP} denotes the second-order derivatives accordingly; d_i represents the EP-to-IP Euclidean distance in the i direction. Once the background field has been determined over the entire VOI, it can be subtracted from the measured field perturbation, ideally leaving only the local field due to tissue susceptibility. We refer to this process as *Extended*-SHARP.

METHODS

E-SHARP Processing

Essential points of the processing scheme are illustrated in Figure 1. For both in vivo and numerical data, the total field (masked, unwrapped, and scaled phase) was SMV filtered (radius = 6 mm), eroded by the radius of the spherical kernel, and finally deconvolved, without regularization, to yield a local *post-SMV* field estimate. The local field estimate was then subtracted from the total field to provide an estimate of the background field over

the reduced brain volume. The hitherto lost EP voxels were paired with their nearest (in the Euclidean sense) IP neighbors for which first and second order spatial derivatives of the background field could be estimated by means of traditional 3-point central differences. For example, for the first derivative in the x-direction:

$$B_x^{\mathrm{IP}}(x_0,y_0,z_0)=\frac{B^{\mathrm{IP}}(x+1,y_0,z_0)-B^{\mathrm{IP}}(x-1,y_0,z_0)}{2\Delta x} \quad [3]$$

where $B^{\mathrm{IP}}(x+1,y_0,z_0)$ and $B^{\mathrm{IP}}(x-1,y_0,z_0)$ are the background field measurements, respectively, one voxel ahead of, and one voxel behind (x_0,y_0,z_0) in the x direction; Δx is the voxel spacing in the x direction. Partial derivatives in y and z were calculated similarly, as were all second order derivatives – determined simply by applying the same 3-point difference scheme to each of the first order partials.

Using these derivatives and the IP-to-EP distances, the background field estimate was extended by means of a second order 3D Taylor expansion (Eq. [2]). The postexpansion background (*extended background* in Fig. 1) was then subtracted from the total field and the truncated singular value decomposition (TSVD) regularization of the original SHARP technique was applied to the result (threshold parameter $\lambda_{\mathrm{TSVD}}=0.05$) (14,28). Specifically, regularization consisted of taking Fourier transforms of the spherical kernel and of the local field estimate; setting to zero the local field Fourier coefficients wherever the magnitude of the corresponding kernel coefficient was less than λ_{TSVD}; and finally taking the inverse Fourier transform of this thresholded form to yield the local field over the extended VOI. In the context of SHARP and E-SHARP, TSVD can be regarded as somewhat analogous to regularizing the deconvolution procedure (Eq. [9] in (14)) with a penalty on the L2 norm of the local field (29). In this way, TSVD offers a convenient means of suppressing undesirable low-frequency components remaining in the local field estimate (30).

In Vivo Experiments

Whole-head 3D multiple gradient echo data were acquired from five volunteers at 4.7 T (Varian, Palo Alto, CA) with the approval of the University of Alberta Research Ethics Board. Acquisition parameters were: field of view = 256 × 160 × 160 mm^3; spatial resolution = 1.0 × 1.0 × 2.0 mm^3; bandwidth = 90.1 kHz; repetition time (TR) = 40 ms; TE = 3/7/11/15/19 ms with unipolar readout; flip angle = 10°. All datasets were processed in MATLAB (version 2012a, The MathWorks, Natick, MA) on a 16-processor computer (Quad-Core Xeon E5620, Intel, Santa Clara, CA) with 46 GB RAM. Images from individual receiver elements (four-channel array) were combined (22) and unwrapped (31), followed by a voxel-wise, magnitude-weighted, least-squares regression of phase to echo time to arrive at the final field maps (32–34).

To obtain a binary brain mask for each dataset, magnitude data from the first echo were passed to FSL's brain extraction tool (BET) (35). Phase discontinuities (jumps to high intensities) were often observed around the outer edges of the mask even after unwrapping. Whether due to shortcomings of Prelude, peculiarities inherent to the data, or the inclusion of nonbrain voxels by an overly generous BET mask, these values were, in any case, deemed unreliable. To define effective brain VOIs that excluded the edge outliers, FSL masks were eroded by between two to four voxels.

Finally, after phase processing, susceptibility maps were formed using the total variation inversion described in (36,37), with the regularization parameter (5×10^{-3}) determined in (29).

Numerical Simulation

A numerical brain model was created by assigning a water-like susceptibility of −9.4 ppm to an in vivo brain mask, while assigning an air-like value of 0 to the region outside the mask. This arrangement was to represent the susceptibility interfaces responsible for the harmonic background field. Although lacking susceptibility structures (e.g., veins and skull) typically associated with a more realistic field map, the simplistic model should suffice insofar as all fields owing to susceptibility sources outside of the brain are in fact harmonic within it, irrespective of the exact distribution of sources. Two *internal* susceptibility inclusions (susceptibility = −9.0 ppm; radii = 2 mm), simulating small spherical hemorrhages, were placed within the brain substrate: one at the center of the brain (IP-region), with the other at the edge (EP-region), such that it would be discarded post-SHARP. The susceptibility model was convolved with the unit dipole field to simulate the magnetic field (16,17), and scaled to phase by the multiplicative factor $\gamma B_0 TE$ ($TE = 19\,\mathrm{ms}$) to which zero-mean Gaussian noise was added (standard deviation = π/4 rad). Model phase quantities are shown in Figure 2a–c. To resemble the common in vivo case, the noisy total phase was masked by the brain VOI before beginning phase processing.

Accuracy of the processing scheme was assessed by means of the relative error between the noiseless model background phase φ_{model} and the background phase estimates φ_{est} given by SHARP and E-SHARP using zeroth, first, and second order expansions:

$$\|M(\varphi_{\mathrm{est}}-\varphi_{\mathrm{model}})\|_2/\|M\varphi_{\mathrm{model}}\|_2. \quad [4]$$

Error terms were ultimately calculated over specific VOIs: for SHARP, the masking operator M was strictly the reduced VOI (IP). For the E-SHARP error calculation, unless otherwise stated, M encompassed the brain VOI (IP + EP), however, as the brain itself does not generally abut air in bulk, M was eroded by a single voxel so as not to contain the outermost voxels that defined the air-tissue interface (where the Laplacian of the background field would be nonzero).

RESULTS

Simulation results are shown for a central slice in Figure 2d–i. The model background field (Fig. 2b) can be seen to be smooth and slowly varying away from transitions in susceptibility and is, therefore, well represented by the second order expansion. Error in the field estimation

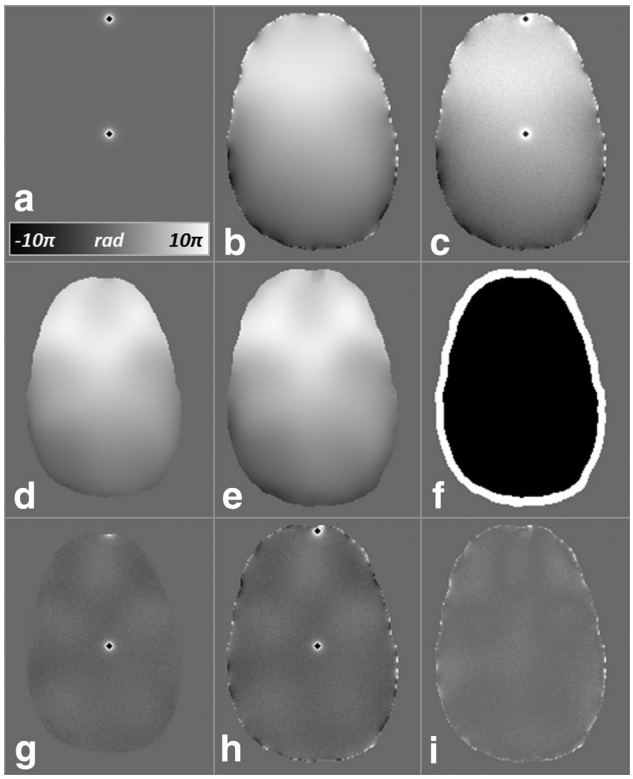

FIG. 2. Numerical simulation. A central transverse slice is shown. The top row corresponds to model phase quantities: local (**a**), masked background (**b**), and noisy total (**c**). **d,e:** The background estimate over the reduced VOI and the full postexpansion form, from SHARP and E-SHARP, respectively. **g,h:** The local phase estimates courtesy of SHARP and E-SHARP, respectively. **i:** The error (absolute difference of (h) and (a)). All images are scaled to the same relative intensities, with the exception of (**f**), which depicts the internal (IP; black) and edge (EP; white) geometries involved.

(Fig. 2i) is greatest in the immediate vicinity of the background source, where the field gradient is steepest. The effect of expansion order on the resulting background phase is illustrated in Figure 3. While relative error was 24% for the zeroth order expansion background phase estimate across the brain VOI (IP+EP), it was reduced to 18%, and further to 16%, for first and second order expansions respectively. Across the reduced VOI alone (not including the EP voxels in M of Eq. [3]), the relative error of E-SHARP (second order expansion) was slightly higher than that of SHARP (15% versus 13%). The corresponding E-SHARP error over the EP voxels alone was 18%.

Example results from a representative in vivo dataset are exhibited in Figure 4. Compared with conventional SHARP, E-SHARP recovered on average 26% more brain volume (values for all five subjects: 27.6%, 27.3%, 27.1%, 25.1%, 25.4%). This additional territory arises from the extension of the reduced VOI of SHARP by the radius of the kernel in all directions, thus revealing cortex and cortical veins (38,39) which were otherwise inaccessible. E-SHARP processing time was on average 3.4 min (range: 1.8–4.3 min).

Susceptibility maps derived from the two methods were similar across the reduced VOI. Representative examples are displayed in Figure 5, with differences shown in the rightmost column. While the SHARP susceptibility map (Fig. 5, left column) exhibited only a reduced portion of the sagittal sinus (middle row) and frontal white matter (top row), the region of susceptibility coverage in these regions was greatly enhanced by E-SHARP (middle column).

DISCUSSION

This study demonstrated that by exploiting the analyticity of the harmonic background field, susceptibility and field maps of comparable quality to those made by conventional SHARP can be achieved with markedly greater spatial support (recovering, on average, 26% more brain volume). Practical considerations concerning the technique are discussed in the following.

First, for the Taylor series to actually equate to the dipole field, it would require, in theory, an infinite number of terms (i.e., derivatives). However, as the background field across the brain is characterized predominantly by the low-order terms, even the truncated form, as observed, can provide satisfactory results in most regions. Furthermore, because the SMV calculation is by definition indifferent to zero-mean Gaussian noise (phase noise in tissue may typically be of this form (21)), the extracted background field is necessarily more or less noise free. This fact, combined with the slow-varying nature of the background field, generally make it

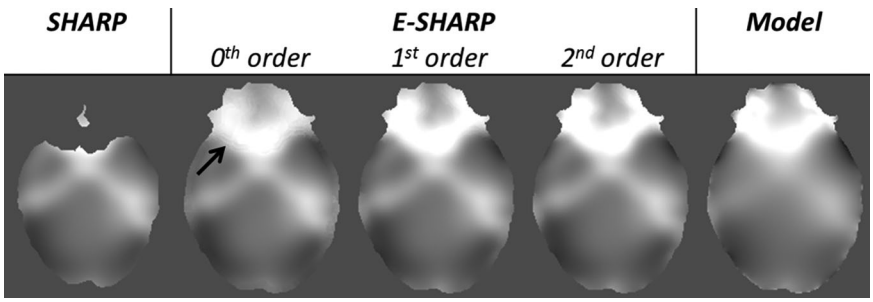

FIG. 3. Effect of order of expansion on the estimated background phase (quantity shown) of the simulated data. Relative error over the reduced VOI was 0.13 for the SHARP background estimate. The corresponding errors were 0.24, 0.18, and 0.16 for zeroth, first, and second order expansions, respectively. As expected, by including higher order terms the discontinuities around the edge (arrow) are smoothed and at second order they are scarcely discernible.

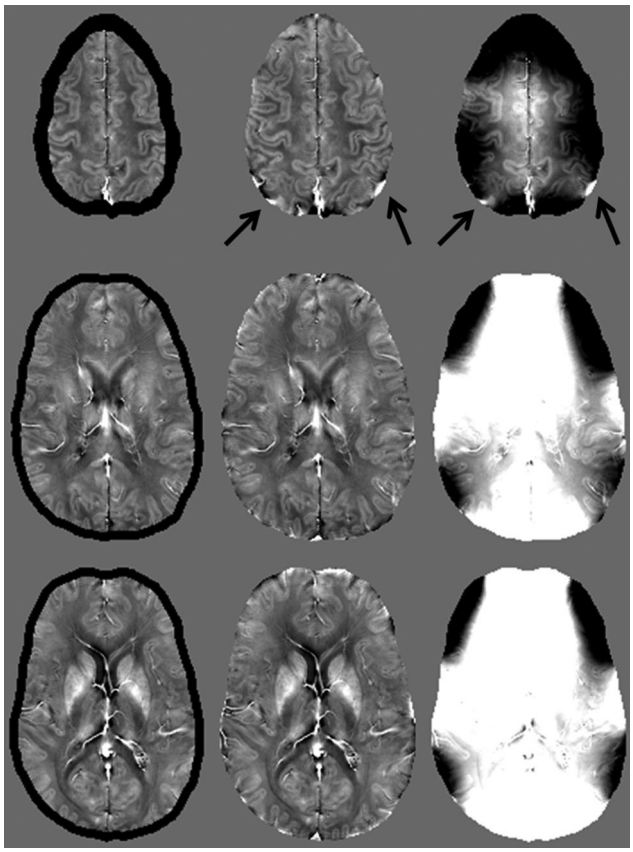

FIG. 4. In vivo results: field processing. From left to right, the columns correspond to the conventional SHARP local field, E-SHARP local field (second order expansion), and total field, respectively. Arrows in the top row point to cortical veins, visible in the total field but lost in conventional SHARP (the black ribbon in the left column demarcates the EP region recovered by E-SHARP).

a fairly safe quantity to subject to otherwise problematic finite-difference calculations.

In terms of series convergence, the second matter of note is the internal point (IP) about which the expansion is performed: in general, the greater the distance d between IP and EP, the more the field will vary between them and, accordingly, the more additional terms in the expansion will be required to compensate. In short, it is beneficial to assign IPs that are as near as possible to the EPs (truncation error being nil only in the limit of $d \to 0$). However, the nature of finite-differences is such that a *difference* between points is required to estimate the derivative: using the 3-point central difference scheme, the first order derivative at x_0 requires field values at x_{+1} and x_{-1}. Given that the input to the expansion (the SMV-estimated background phase) has finite spatial support (the reduced VOI), we cannot calculate a first derivative directly at the edge of support, but rather one voxel removed from it; likewise, the nearest point to the edge of support at which we can calculate a second derivative is two voxels removed from it. In this way, by increasing the order of the expansion, so too must d be increased, which in some sense confounds convergence. Nevertheless, for the numerical simulation, the lowest relative error was observed for the second order expansion (16%). Thus, for the particular model field studied, the inclusion of higher order terms proved to be of greater benefit than the adoption of IPs that were slightly more proximal to the EPs.

Third, the quoted results depend intimately on the adopted parameters. For instance, as the error calculations incorporated the entire EP region, calculated errors were governed, not only by the order of expansion, but also by its particular geometry. A key factor in the determination of this geometry was the size of spherical kernel – a parameter that merits further study in its own right. So too does the regularization parameter (28). Indeed, before regularization, the post-SMV local field estimate over the reduced VOI is identical between SHARP and E-SHARP and it is only subsequent to SHARP-style TSVD that there is a subtle (Fig. 3) but, nevertheless, calculable difference (2% more error with E-SHARP) in this internal region. Ultimately, this may simply suggest that optimal SHARP parameters may not translate into optimal E-SHARP parameters. A more complete treatment of the interplay between these parameters, however, is beyond the scope of this work, for which the aim has been simply to demonstrate that by means of a slight modification to conventional SHARP one can arrive at a local field map with substantially expanded spatial support (e.g., Fig. 4).

Finally, although E-SHARP revealed extensive new territory, a portion of the edge remained missing due to the naïve correction applied to the initial brain mask. The sagittal view of the susceptibility maps (Fig. 5, middle row) evinces this issue. Because the removal of erroneous phase outliers was achieved at the expense of retaining the full brain VOI, parts of the edge region were

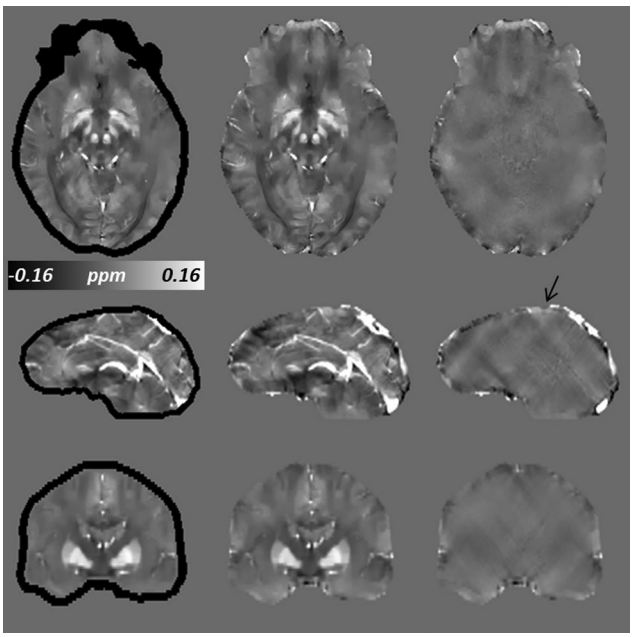

FIG. 5. In vivo results: QSM. Columns correspond to the susceptibility maps formed using SHARP (left) for the phase processing and E-SHARP (center). Again, the black ribbon in the left column demarcates the EP region recovered by E-SHARP. The difference is shown in the rightmost column, with the arrow in the middle row pointing to the artificial truncation of the sagittal sinus due to the naïve initial correction applied to the brain mask.

erroneously truncated (e.g., the sagittal sinus; arrow in Fig. 5, right column). To solve this issue and retain the brain VOI to its fullest, a means of automatic detection and exclusion of problematic phase data will ultimately be required.

CONCLUSIONS

Extended-SHARP—an easily implemented adaptation to the postprocessing technique SHARP—can be used to determine the subset of missing field map values around the edges of the brain. Results suggest a new way of processing MR phase that may bring us one step closer to a reliable technique for whole-brain in vivo susceptibility assessment.

ACKNOWLEDGMENTS

This work was made possible through funding from the Canadian Institutes of Health Research (CIHR), the Natural Sciences and Engineering Research Council of Canada (NSERC), the German Research Foundation (DFG), a seed grant awarded to A.D. by the Interdisciplinary Center for Clinical Research (IZKF) in Jena, Germany, seed grants awarded to F.S. by the International Society for Magnetic Resonance in Medicine (ISMRM) and the Friedrich Schiller University Jena, and a Queen Elizabeth II Graduate Scholarship awarded to R.T. by the University of Alberta.

REFERENCES

1. Reichenbach JR, Venkatesan R, Schillinger DJ, Kido DK, Haacke EM. Small vessels in the human brain: MR venography with deoxyhemoglobin as an intrinsic contrast agent. Radiology 1997;204:272–277.
2. Wang Y, Yu Y, Li D, Bae KT, Brown JJ, Lin W, Haacke EM. Artery and vein separation using susceptibility-dependent phase in contrast-enhanced MRA. J Magn Reson Imaging 2000;12:661–670.
3. Reichenbach JR, Haacke EM. High-resolution BOLD venographic imaging: a window into brain function. NMR Biomed 2001;14:453–467.
4. Haacke EM, Xu Y, Cheng Y-CN, Reichenbach JR. Susceptibility weighted imaging (SWI). Magn Reson Med 2004;52:612–618.
5. Deistung A, Mentzel HJ, Rauscher A, Witoszynskyj S, Kaiser WA, Reichenbach JR. Demonstration of paramagnetic and diamagnetic cerebral lesions by using susceptibility weighted phase imaging (SWI). Z Med Phys 2006;16:261–267.
6. Shmueli K, de Zwart JA, van Gelderen P, Li TQ, Dodd SJ, Duyn JH. Magnetic susceptibility mapping of brain tissue in vivo using MRI phase data. Magn Reson Med 2009;62:1510–1522.
7. De Rochefort L, Liu T, Kressler B, Liu J, Spincemaille P, Lebon V, Wu J, Wang Y. Quantitative susceptibility map reconstruction from MR phase data using Bayesian regularization: validation and application to brain imaging. Magn Reson Med 2010;63:194–206.
8. Li W, Wu B, Liu C. Quantitative susceptibility mapping of human brain reflects spatial variation in tissue composition. Neuroimage 2011;55:1645–1656.
9. Schweser F, Sommer K, Deistung A, Reichenbach JR. Quantitative susceptibility mapping for investigating subtle susceptibility variations in the human brain. Neuroimage 2012;62:2083–2100.
10. Deistung A, Schafer A, Schweser F, Biedermann U, Turner R, Reichenbach JR. Toward in vivo histology: a comparison of quantitative susceptibility mapping (QSM) with magnitude-, phase-, and R2*-imaging at ultra-high magnetic field strength. Neuroimage 2013;65:299–314.
11. Reichenbach JR. The future of susceptibility contrast for assessment of anatomy and function. Neuroimage 2012;62:1311–1315.
12. Sadrzadeh SMH, Saffari Y. Iron and brain disorders. (Pathology Patterns Rev. S64) Am J Clin Pathol 2004;121:65–70.
13. Schenck JF. The role of magnetic susceptibility in magnetic resonance imaging: MRI magnetic compatibility of the first and second kinds. Med Phys 1996;23:815–850.
14. Schweser F, Deistung A, Lehr BW, Reichenbach JR. Quantitative imaging of intrinsic magnetic tissue properties using MRI signal phase: an approach to in vivo brain iron metabolism? Neuroimage 2011;54:2789–807.
15. Liu T, Khalidov I, de Rochefort L, Spincemaille P, Liu J, Tsiouris AJ, Wang Y. A novel background field removal method for MRI using projection onto dipole fields (PDF). NMR Biomed 2011;24:1129–1136.
16. Salomir R, de Senneville BD, Moonen CT. A fast calculation method for magnetic field inhomogeneity due to an arbitrary distribution of bulk susceptibility. Concepts Magn Reson 2003;19B:26–34.
17. Marques JP, Bowtell R. Application of a Fourier-based method for rapid calculation of field inhomogeneity due to spatial variation of magnetic susceptibility. Concepts Magn Reson Part B Magn Reson Eng 2005;25B:65–78.
18. Richards PI. Manual of mathematical physics. Belfast: Pergamon Press Ltd; 1959. p 316–317.
19. Topfer R, Schweser F, Deistung A, Wilman AH, Reichenbach JR. SHARP edges: recovering cortical phase contrast through harmonic extension. In Proceedings of the 21st Annual Meeting of ISMRM, Salt Lake City, Utah, USA, 2013. Abstract 3856.
20. Li L, Leigh JS. High-precision mapping of the magnetic field utilizing the harmonic function mean value property. J Magn Reson 2001;148:442–448.
21. Gudbjartsson H, Patz S. The Rician distribution of noisy MRI data. Magn Reson Med 1995;34:910–914.
22. Robinson S, Grabner G, Witoszynskyj S, Trattnig S. Combining phase images from multi-channel RF coils using 3D phase offset maps derived from a dual-echo scan. Magn Reson Med 2011;65:1638–1648.
23. Chu SC, Xu Y, Balschi JA, Springer CS. Bulk magnetic susceptibility shifts in NMR studies of compartmentalized samples: use of paramagnetic reagents. Magn Reson Med 1990;13:239–262.
24. Luo J, He X, D'Avignon DA, Ackerman JJH, Yablonskiy DA. Protein-induced water 1H MR frequency shifts: contributions from magnetic susceptibility and exchange effects. J Magn Reson 2010;202:102–108.
25. Shmueli K, Dodd SJ, Li T-Q, Duyn JH. The contribution of chemical exchange to MRI frequency shifts in brain tissue. Magn Reson Med 2011;65:35–43.
26. Leutritz T, Hilfert L, Smalla K-H, Speck O, Zhong K. Accurate quantification of water-macromolecule exchange induced frequency shift: effects of reference substance. Magn Reson Med 2013;69:263–268.
27. Roy KK. Green's theorem in potential theory. In: Potential theory in applied geophysics. Berlin: Springer; 2008. p 307–328.
28. Schweser F, Sommer K, Atterbury M, Deistung A, Lehr BW, Reichenbach JR. On the impact of regularization and kernel type on SHARP-corrected GRE phase images. In Proceedings of the 19th Annual Meeting of ISMRM, Montreal, Canada, 2011. Abstract 5165.
29. Sun H, Wilman AH. Background field removal using spherical mean value filtering and Tikhonov regularization. Magn Reson Med 2014;71:1151–1157.
30. Schweser F, Atterbury M, Deistung A, Lehr BW, Sommer K, Reichenbach JR. Harmonic phase subtraction methods are prone to B 1 background components. In Proceedings of the 19th Annual Meeting of ISMRM, Montreal, Canada, 2011. Abstract 2657.
31. Jenkinson M. Fast, automated, N-dimensional phase-unwrapping algorithm. Magn Reson Med 2003;49:193–197.
32. Gilbert G, Savard G, Bard C, Beaudoin G. Quantitative comparison between a multiecho sequence and a single-echo sequence for susceptibility-weighted phase imaging. Magn Reson Imaging 2012;30:722–730.
33. Wu B, Li W, Avram AV, Gho S-M, Liu C. Fast and tissue-optimized mapping of magnetic susceptibility and T2* with multi-echo and multi-shot spirals. Neuroimage 2012;59:297–305.
34. Denk C, Rauscher A. Susceptibility weighted imaging with multiple echoes. J Magn Reson Imaging 2010;31:185–191.
35. Smith SM. Fast robust automated brain extraction. Hum Brain Mapp 2002;17:143–155.
36. Lustig M, Donoho D, Pauly JM. Sparse MRI: the application of compressed sensing for rapid MR imaging. Magn Reson Med 2007;58:1182–1195.
37. Wu B, Li W, Guidon A, Liu C. Whole brain susceptibility mapping using compressed sensing. Magn Reson Med 2012;67:137–147.
38. Agid R, Shelef I, Scott JN, Farb RI. Imaging of the intracranial venous system. Neurologist 2008;14:12–22.
39. Fan AP, Bilgic B, Gagnon L, Witzel T, Bhat H, Rosen BR, Adalsteinsson E. Quantitative oxygenation venography from MRI phase. Magn Reson Med 2013. doi: 10.1002/mrm.24918.